Int J Thermophys (2008) 29:2102–2115
DOI 10.1007/s10765-007-0261-4

Metrological Aspects of Auto-normalized Front Photopyroelectric Method to Measure Thermal Effusivity in Liquids

G. Gutiérrez-Juárez · R. Ivanov · J. P. Pichardo-Molina · M. Vargas-Luna · J. J. Alvarado-Gil · A. Camacho

Published online: 21 September 2007

Abstract The metrological aspects related to the sensitivity and signal-to-noise ratio of the auto-normalized front pyroelectric technique for the measurement of thermal effusivity in liquids are investigated. The effect of the thermally thick approximation in the theoretical expressions for the photopyroelectric signal and its effect on the sensitivity of the technique are discussed. It is shown that the sensitivity of the technique decreases with frequency. In contrast, the signal-to-noise ratio increases for higher frequencies.

Keywords Photopyroelectric technique · Sensitivity · Signal-to-noise ratio · Thermal effusivity

G. Gutiérrez-Juárez (✉) · M. Vargas-Luna
Instituto de Física de la Universidad de Guanajuato, Loma del bosque 103, Lomas del Campestre, Leon, Gto, C.P. 37150, México
e-mail: ggutj@fisica.ugto.mx

R. Ivanov
Facultad de Física, Universidad Autónoma de Zacatecas, Av. Preparatoria 301, Col. Progreso, Zacatecas, Zac., C.P. 98060, México

J. P. Pichardo-Molina
Centro de Investigaciones en Óptica, Loma del Bosque 115, Lomas del Campestre, Leon, Gto, C.P. 37150, México

J. J. Alvarado-Gil
Departamento de Física Aplicada, CINVESTAV- Mérida, Cordemex , Merida, Yuc, C.P. 97310, México

A. Camacho
Universidad Tecnológica de León, Blvd. Universidad Tecnológica 225, San Carlos, Leon, Gto, 37670, México

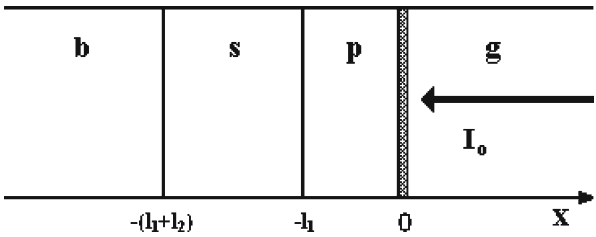

Fig. 1 Geometry of the conventional FPPE cell. Here, g is air, p is the pyroelectric sensor of thickness l_1, s is the sample of thickness l_2, and b is the backing material. I_0 is the intensity of the incident modulated light beam impinging onto the pyroelectric sensor at $x = 0$

1 Introduction

During the last decade the photothermal (PT) technique has been extensively applied to the study of thermal properties of solids and liquid samples [1–4]. Among the PT techniques, the photopyroelectric method has been shown to be a reliable technique for the thermal characterization of samples with very good thermal contact with the sensor (liquids mainly). The photopyroelectric technique (PPE) consists essentially of a pyroelectric sensor in perfect contact with the sample under study. There are two configurations of the PPE technique, in the first one; known as the back photopyroelectric technique (BPPE), the sample is on top of the pyroelectric sensor and is illuminated directly by a modulated light beam.

The second is named the front photopyroelectric technique (FPPE); in this modality, the modulated light beam illuminates the pyroelectric sensor, causing periodic heating that is transmitted to the sample. The heating produces an electric current that carries information on the thermal diffusivity (α) and thermal effusivity (e) of the sample [5,6].

The determination of the thermal parameters with the PPE technique is performed by fitting the experimental data using an adequate photothermal model.

The present work is focused on the theory of the FPPE technique, and explores the sensitivity of the technique. For this purpose, the sensitivity of the technique is defined as the variation of the signal when the thermophysical parameters of the sample are varied.

2 Theory

2.1 FPPE Temperature Field

A sketch of the conventional FPPE cell is shown in Fig. 1. Here, g is air, p is the pyroelectric sensor of thickness l_1, s is the sample of thickness l_2, and b is the backing material. I_0 is the intensity of the incident modulated light beam, which impinges onto the pyroelectric sensor at $x = 0$.

It has been shown that the PPE signal, in the voltage or current mode, is proportional to the average temperature in the pyroelectric sensor, $\langle T(t, \omega)\rangle$ [1,2], which is given

by

$$\left\langle T_p\left(t,\omega\right)\right\rangle = \left[\frac{1}{l_1}\int_{-l_1}^{0} T_p\left(x\right)\mathrm{d}x\right]\exp\left(i\omega t\right), \tag{1}$$

where $\omega = 2\pi f$, with f the chopping frequency of the incident radiation and $T_p(x)$ the temperature along the pyroelectric sensor. In order to obtain this temperature, we have to solve the following system of thermal diffusion equations:

$$\frac{\mathrm{d}^2 T_j\left(x\right)}{\mathrm{d}x^2} - \frac{i\omega}{\alpha_j}T_j\left(x\right) = 0; \quad j = g,\ p,\ s,\ b \tag{2}$$

Assuming that the sensor is optically opaque, in such a way that the radiation is completely absorbed at the front surface of the sensor, the boundary conditions are

$$\begin{aligned} &T_i\left(\text{boundary}\right) = T_j\left(\text{boundary}\right) && (i,j) = (g,p);\ (p,s);\ (s,b)\\ &k_i\frac{\mathrm{d}T_j(x)}{\mathrm{d}x} - k_j\frac{\mathrm{d}T_j(x)}{\mathrm{d}x} = \begin{cases} 0 \\ \\ \frac{1-R}{2}I_0 \end{cases}; && \begin{matrix}(i,j) = (p,s);\ (s,p)\\ (i,j) = (g,p)\end{matrix} \end{aligned} \tag{3}$$

In Eqs. 1–3, $T_i(x,t) = T_i(x)\exp(i\omega t)$, $I(t) = I_0\exp(i\omega t)$, α_i and k_i are the thermal diffusivity and thermal conductivity of the i-th component of the cell, R is the fraction of radiation reflected by the electrode of the sensor, and $I(t)$ is the intensity of the modulated light beam.

Solving Eqs. 1–3, the average temperature in the pyroelectric sensor is obtained;

$$\left\langle T_{\mathrm{p}}\left(t,\omega\right)\right\rangle = I_{\mathrm{o}}\left(1-R\right)\frac{\left(1+R_{\mathrm{gp}}\right)}{4k_{\mathrm{p}}\sigma_{\mathrm{p}}}\Gamma\,\exp\left(i\omega t\right) \tag{4}$$

where

$$\Gamma = \frac{\left(1-\mathrm{e}^{-\sigma_{\mathrm{p}}l_1}\right)}{\sigma_{\mathrm{p}}l_1}\left[\frac{\left(R_{\mathrm{sp}}+R_{\mathrm{bs}}\mathrm{e}^{-2\sigma_{\mathrm{s}}l_2}\right)\mathrm{e}^{-\sigma_{\mathrm{p}}l_1}+\left(1+R_{\mathrm{sp}}R_{\mathrm{bs}}\mathrm{e}^{-2\sigma_{\mathrm{s}}l_2}\right)}{R_{\mathrm{gp}}\mathrm{e}^{-2\sigma_{\mathrm{p}}l_1}\left(R_{\mathrm{sp}}+R_{\mathrm{bs}}\mathrm{e}^{-2\sigma_{\mathrm{s}}l_2}\right)-\left(1+R_{\mathrm{sp}}R_{\mathrm{bs}}\mathrm{e}^{-2\sigma_{\mathrm{s}}l_2}\right)}\right] \tag{5}$$

In Eq. 5 the following notation has been used:

$$R_{ij} = \frac{1-b_{ij}}{1+b_{ij}},\quad b_{ij} = \frac{e_i}{e_j},\quad \sigma_j = (1+i)\,a_j,\quad a_j^{-1} = \mu_j = \sqrt{\frac{\alpha_j}{\pi f}}.$$

where μ_j is the so-called thermal diffusion length.

If the sample is air (s = g), the expression for Γ is reduced to

$$\Gamma_{\mathrm{g}} = \frac{1}{\sigma_{\mathrm{p}}l_1}\frac{\left(1-\mathrm{e}^{-\sigma_{\mathrm{p}}l_1}\right)\left(R_{\mathrm{sp}}\mathrm{e}^{-\sigma_{\mathrm{p}}l_1}+1\right)}{\left(R_{\mathrm{gp}}^2\mathrm{e}^{-2\sigma_{\mathrm{p}}l_1}-1\right)} = \frac{1}{\sigma_{\mathrm{p}}l_1}\frac{\left(1-\mathrm{e}^{-\sigma_{\mathrm{p}}l_1}\right)}{\left(R_{\mathrm{gp}}\mathrm{e}^{-\sigma_{\mathrm{p}}l_1}-1\right)} \tag{6}$$

which is obtained from Eq. 5 making the change s → g in the subscripts and making the exponential $\exp(-2\sigma_s l_2)$ equal to zero. Combining Eqs. 5 and 6, the following equation is obtained:

$$\Gamma = \Gamma_g \left(R_{gp} e^{-\sigma_p l_1} - 1\right) \left[\frac{\left(R_{sp} + R_{bs} e^{-2\sigma_s l_2}\right) e^{-\sigma_p l_1} + \left(1 + R_{sp} R_{bs} e^{-2\sigma_s l_2}\right)}{R_{gp}\left(R_{sp} + R_{bs} e^{-2\sigma_s l_2}\right) e^{-2\sigma_p l_1} - \left(1 + R_{sp} R_{bs} e^{-2\sigma_s l_2}\right)}\right],$$

and after some calculations,

$$\Gamma = \Gamma_g \left[1 + \frac{\left(R_{sp} + R_{bs} e^{-2\sigma_s l_2}\right) - R_{gp}\left(1 + R_{sp} R_{bs} e^{-2\sigma_s l_2}\right)}{\left(1 + R_{sp} R_{bs} e^{-2\sigma_s l_2}\right) e^{\sigma_p l_1} - R_{gp}\left(R_{sp} + R_{bs} e^{-2\sigma_s l_2}\right) e^{-\sigma_p l_1}}\right],$$

then the average temperature, for the configuration given in Fig. 1, can be rewritten as follows:

$$\left\langle T_p(t,\omega)\right\rangle = \left[1 + \frac{\left(R_{sp} - R_{gp}\right) - R_{bs}\left(1 + R_{sp} R_{gp}\right) e^{-2\sigma_s l_2}}{\left(1 + R_{sp} R_{bs} e^{-2\sigma_s l_2}\right) e^{\sigma_p l_1} - R_{gp}\left(R_{sp} + R_{bs} e^{-2\sigma_s l_2}\right) e^{-\sigma_p l_1}}\right] \left\langle T_g(t,\omega)\right\rangle, \tag{7}$$

where

$$\left\langle T_g(t,\omega)\right\rangle = \frac{I_o(1-R)\left(1+R_{gp}\right)}{4 l_p k_p \sigma_p^2} \left(\frac{1 - e^{-\sigma_p l_1}}{R_{gp} e^{-\sigma_p l_1} - 1}\right) \exp(i\omega t) \tag{8}$$

is the average temperature for the sensor alone. As can be seen in Eq. 8, $\left\langle T_p(t,\omega)\right\rangle$ is only a function of two thermal parameters of the sample, e_s through R_{bs} and α_s through σ_s.

2.2 FPPE Signal

It has been shown [1] that the average pyroelectric voltage is given by

$$V = \frac{\langle Q\rangle}{C} = \frac{p}{C}\langle T(t,\omega)\rangle, \tag{9}$$

where C and p are the capacitance per unit area and the pyroelectric coefficient of the pyroelectric thin film, respectively.

Due to the fact that a pyroelectric sensor can be considered as a capacitor of two parallel charged plates of thickness l_1, then the voltage generated in the pyroelectric sensor is

$$V = \frac{p l_1}{K \varepsilon_0}\langle T(t,\omega)\rangle, \tag{10}$$

where ε_0 is the permittivity constant of vacuum.

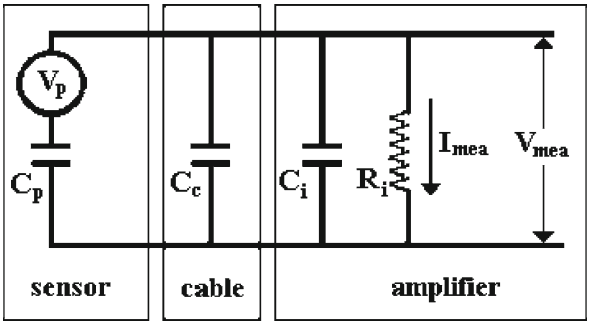

Fig. 2 Equivalent circuit for the pyroelectric sensor, cable, and lock-in amplifier

Substituting Eqs. 7 and 8 in Eq. 10, the voltage generated in the pyroelectric sensor is

$$V = V_{\mathrm{g}} \left[1 + \frac{\left(R_{\mathrm{sp}} - R_{\mathrm{gp}}\right) - R_{\mathrm{bs}} \left(1 + R_{\mathrm{sp}} R_{\mathrm{gp}}\right) \mathrm{e}^{-2\sigma_{\mathrm{s}} l_2}}{\left(1 + R_{\mathrm{sp}} R_{\mathrm{bs}} e^{-2\sigma_{\mathrm{s}} l_2}\right) \mathrm{e}^{\sigma_{\mathrm{p}} l_1} - R_{\mathrm{gp}} \left(R_{\mathrm{sp}} + R_{\mathrm{bs}} \mathrm{e}^{-2\sigma_{\mathrm{s}} l_2}\right) \mathrm{e}^{-\sigma_{\mathrm{p}} l_1}} \right], \tag{11}$$

where

$$V_{\mathrm{g}} = \frac{p l_1}{K \varepsilon_{\mathrm{o}}} \left\langle T_{\mathrm{g}} \left(t, \omega\right) \right\rangle$$

is the voltage generated in the pyroelectric without a sample.

In order to obtain the function for the measured voltage or current, the equivalent circuit given in Fig. 2 is used [7]. In this equivalent circuit, V_{p} is a voltage generator, which in our case is given by Eq. 11. The reason for using this circuit is due to the fact that at low frequencies, there are practically no losses at the pyroelectric sensor (or the cable and input preamplifier).

2.2.1 Voltage Mode of the FPPE Signal

The equivalent circuit of the ideal voltage mode is shown in Fig. 2. In this sketch $C_{\mathrm{k}} = C_{\mathrm{c}} + C_{\mathrm{i}}$ is the resultant capacitance of cable and input preamplifier capacitances, which are in parallel. Applying Kirchhoff laws, we obtain

$$V_{\mathrm{mea}} = \frac{C}{C + C_{\mathrm{k}}} V. \tag{12}$$

Substituting Eq. 12 in Eq. 11, we get

$$V_{\mathrm{mea}} = V_{\mathrm{gmea}} \left[1 + \frac{\left(R_{\mathrm{sp}} - R_{\mathrm{gp}}\right) - R_{\mathrm{bs}} \left(1 + R_{\mathrm{sp}} R_{\mathrm{gp}}\right) \mathrm{e}^{-2\sigma_{\mathrm{s}} l_2}}{\left(1 + R_{\mathrm{sp}} R_{\mathrm{bs}} \mathrm{e}^{-2\sigma_{\mathrm{s}} l_2}\right) \mathrm{e}^{\sigma_{\mathrm{p}} l_1} - R_{\mathrm{gp}} \left(R_{\mathrm{sp}} + R_{\mathrm{bs}} \mathrm{e}^{-2\sigma_{\mathrm{s}} l_2}\right) \mathrm{e}^{-\sigma_{\mathrm{p}} l_1}} \right] \tag{13}$$

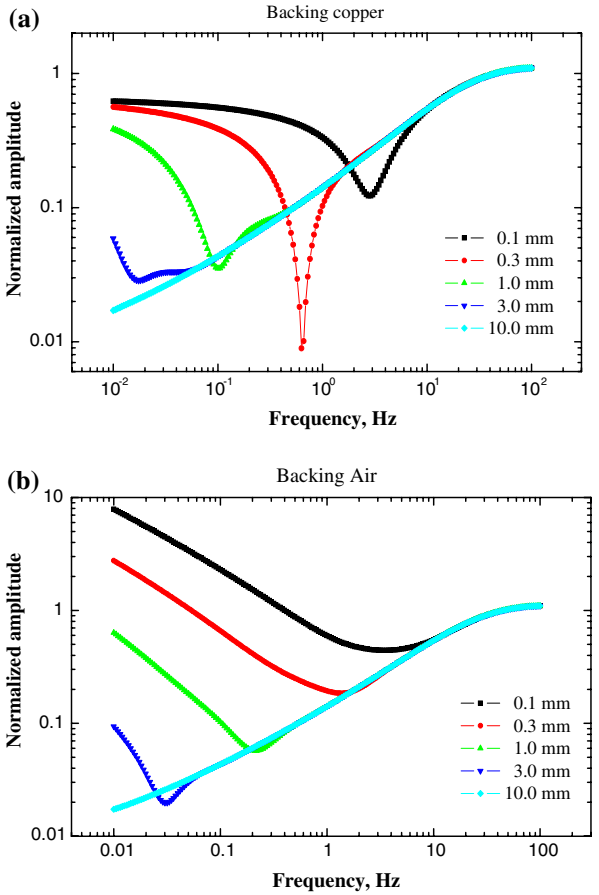

Fig. 3 Normalized amplitude signal of FPPE mode for water using (**a**) copper and (**b**) air as backing materials

where

$$V_{\mathrm{gmea}} = \frac{p}{C + C_{\mathrm{k}}} \left\langle T_{\mathrm{g}}\left(t, \omega\right)\right\rangle$$

2.2.2 Current Mode of the FPPE Signal

Applying Kirchhoff laws to the circuit in Fig. 2, it can be shown that

$$I_{\mathrm{mea}} = i\omega C V. \tag{14}$$

Substituting Eq. 11 in Eq. 14, we get

$$I_{\text{mea}} = I_{\text{gmea}} \left[1 + \frac{\left(R_{\text{sp}} - R_{\text{gp}}\right) - R_{\text{bs}} \left(1 + R_{\text{sp}} R_{\text{gp}}\right) \mathrm{e}^{-2\sigma_{\text{s}} l_2}}{\left(1 + R_{\text{sp}} R_{\text{bs}} \mathrm{e}^{-2\sigma_{\text{s}} l_2}\right) \mathrm{e}^{\sigma_{\text{p}} l_1} - R_{\text{gp}} \left(R_{\text{sp}} + R_{\text{bs}} \mathrm{e}^{-2\sigma_{\text{s}} l_2}\right) \mathrm{e}^{-\sigma_{\text{p}} l_1}} \right], \tag{15}$$

where $I_{\text{gmea}} = i\omega C V_{\text{g}}$.

3 Numerical Evaluation

Normalizing Eq. 13 or 15 with their respective FPPE signal of the sensor without a sample, it can be shown that

$$q = \frac{S_{\text{mea}}}{S_{\text{gmea}}} = 1 + \frac{\left(R_{\text{sp}} - R_{\text{gp}}\right) - R_{\text{bs}} \left(1 + R_{\text{sp}} R_{\text{gp}}\right) \mathrm{e}^{-2\sigma_{\text{s}} l_2}}{\left(1 + R_{\text{sp}} R_{\text{bs}} \mathrm{e}^{-2\sigma_{\text{s}} l_2}\right) \mathrm{e}^{\sigma_{\text{p}} l_1} - R_{\text{gp}} \mathrm{e}^{-\sigma_{\text{p}} l_1} \left(R_{\text{sp}} + R_{\text{bs}} \mathrm{e}^{-2\sigma_{\text{s}} l_2}\right)}, \tag{16}$$

where S_{mea} is the measured FPPE signal and S_{gmea} is the signal measured by the pyroelectric sensor without a sample. From the point of view of the thermal properties of the sample, q is a function of just two thermal parameters, namely, the thermal effusivity and thermal diffusivity.

In order to analyze the behavior of q, numerical simulation of a water sample was performed for five different thicknesses ($l_2 = 0.1$, 0.3, 1.0, 3.0, and 10.0 mm). The water thermal properties were taken as $\alpha_{\text{w}} = 0.145 \times 10^{-6}\ \text{m}^2 \cdot \text{s}^{-1}$ and $e_{\text{w}} = 1,600.000\ \text{W} \cdot \text{s}^{1/2} \cdot \text{m}^{-2} \cdot \text{K}^{-1}$ [8]. Two types of backings were considered: air ($\alpha_{\text{g}} = 22.260 \times 10^{-6}\ \text{m}^2 \cdot \text{s}^{-1}$, $e_{\text{g}} = 5.510\ \text{W} \cdot \text{s}^{1/2} \cdot \text{m}^{-2} \cdot \text{K}^{-1}$) and copper ($\alpha_{\text{c}} = 96.800 \times 10^{-6}\ \text{m}^2 \cdot \text{s}^{-1}$, $e_{\text{c}} = 2.409 \times 10^{4}\ \text{W} \cdot \text{s}^{1/2} \cdot \text{m}^{-2} \cdot \text{K}^{-1}$) [8]. The thermal parameters used for the pyroelectric sensor are $\alpha_{\text{p}} = 0.065 \times 10^{-6}\ \text{m}^2 \cdot \text{s}^{-1}$, and $e_{\text{p}} = 609.900\ \text{W} \cdot \text{s}^{1/2} \cdot \text{m}^{-2} \cdot \text{K}^{-1}$ [9], with $l_1 = 30\ \mu$m. The frequency range was varied from 0.01 to 100 Hz.

Figure 3 show the behavior of the normalized amplitudes q, and Fig. 4 shows the behavior of their phase (see Eq. 16). It can be observed that, even though the thermal diffusion length of water is 2.15 mm at 0.01 Hz, the effect of the backing disappears when the thickness of the sample is approximately four times the thermal diffusion length (10 mm).

3.1 Thermally Thick Samples

This section is devoted to the analysis of thermally thick samples, and to a comparison of the simulations of this approximation with the results obtained using the complete expression. The normalized expression for thermally thick samples can be written as

$$q = 1 + \frac{\left(R_{\text{sp}} - R_{\text{gp}}\right)}{\mathrm{e}^{\sigma_{\text{p}} l_1} - R_{\text{sp}} R_{\text{gp}} \mathrm{e}^{-\sigma_{\text{p}} l_1}}. \tag{17}$$

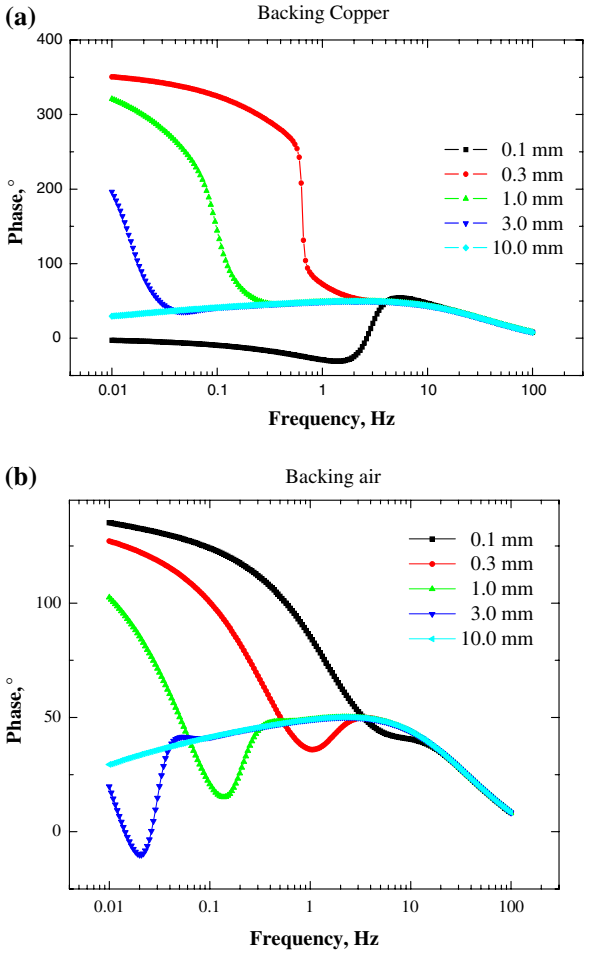

Fig. 4 Normalized phase signal of FPPE mode for water as a sample with different thicknesses and using (**a**) copper and (**b**) air as backing material

It can be observed in this equation that the FPPE signal does not depend on the thermal diffusivity of the sample as is the case of the complete expression (Eq. 16) and that only the dependence on the thermal effusivity of the sample remains. Writing Eq. 17 in terms of amplitude and phase, the following results are obtained:

$$|q| = \sqrt{1 + (R_{sp} - R_{gp}) \left[\frac{(2\cos x)\, e^{-x} + (R_{sp} - R_{gp})\, e^{-2x} - (2R_{sp}R_{gp}\cos x)\, e^{-3x}}{1 - (2R_{sp}R_{gp}\cos 2x)\, e^{-2x} + R_{sp}^2 R_{gp}^2 e^{-4x}}, \right]} \tag{18}$$

and

$$\phi_q = \arctan\left[\frac{\left(e^x + R_{sp}R_{gp}e^{-x}\right)\sin x}{\left(R_{sp} - R_{gp}\right) + \left(e^x - R_{sp}R_{gp}e^{-x}\right)\cos x}\right] - \arctan\left[\frac{\left(1 + R_{sp}R_{gp}e^{-2x}\right)}{\left(1 - R_{sp}R_{gp}e^{-2x}\right)}\tan x\right].$$

In these equations, $x = a_p l_1$.

In order to compare the difference between the complete signal and the approximation for thermally thick samples, in Fig. 5, the amplitude and phase using Eqs. 16 and 18, for two backings, copper and air, with a sample with a thickness of 3 mm are shown. It can be observed that there are no significant differences for frequencies from 0.1 to 100 Hz. This can be verified by calculating the relative difference between the amplitude of the signals and the difference between the phases. The relative difference between the amplitudes is given by

$$\eta = \left(1 - \frac{|q_{app}|}{|q_{exac}|}\right) \times 100.$$

As can be seen in Fig. 6, there are practically no differences between complete and approximated FPPE signals, for frequencies above 0.2 Hz. The amplitude is nearly the same, and the phase shows a very small difference (0.3°). The difference between the complete expression for q and the thermally thick approximation for a sample of 10 mm is minimal over the range of frequencies above 0.1 Hz.

4 Sensitivity

With the purpose of showing that the auto-normalized FPPE technique is a reliable technique, in this section the sensitivity to small changes in the thermal properties is explored. First, we analyze the variation of the signal, Δq, when the thermal effusivity e_s and thermal diffusivity α_s are changed by a quantity Δe_s and $\Delta\alpha_s$, respectively. Therefore,

$$\Delta q = \left(\frac{\partial q}{\partial e_s}\right)\Delta e_s + \left(\frac{\partial q}{\partial \alpha_s}\right)\Delta \alpha_s$$

Due to the fact that q is a function of e_s through R_{sp} and R_{bs}, and is a function of α_s through σ_s, the following equations can be written:

$$\frac{\partial q}{\partial e_s} = \frac{\partial q}{\partial R_{sp}}\frac{\partial R_{sp}}{\partial e_s} + \frac{\partial q}{\partial R_{bs}}\frac{\partial R_{bs}}{\partial e_s} \quad \text{and} \quad \frac{\partial q}{\partial \alpha_s} = \frac{\partial q}{\partial \sigma_s}\frac{\partial \sigma_s}{\partial \alpha_s}.$$

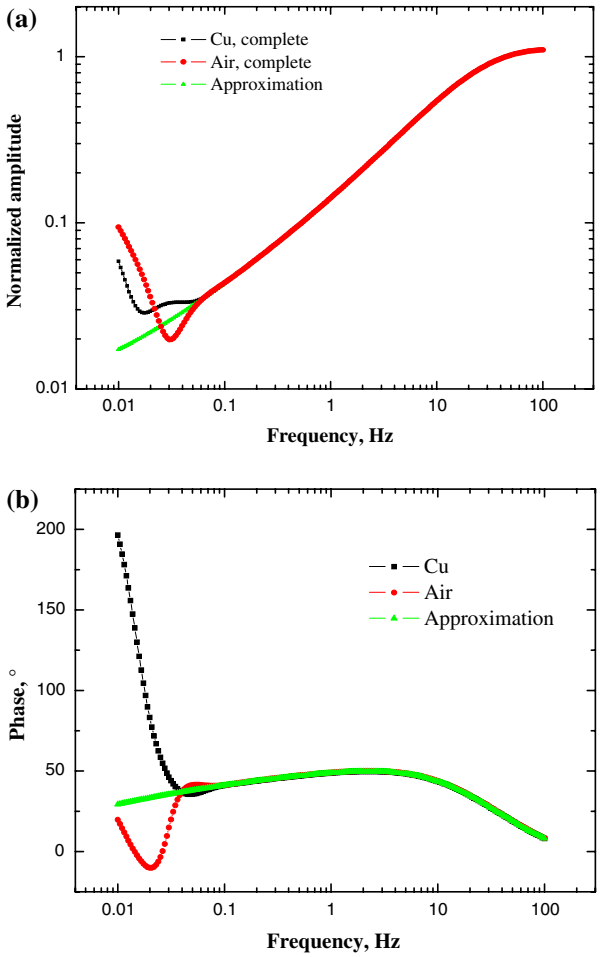

Fig. 5 Comparison between the complete FPPE signal and the thermally thick approximation for water sample of 3 mm thickness: (**a**) amplitude q and (**b**) phase. Above 0.1 Hz, the backing influence (air or copper) is minimal

From the definition of R_{ij}, b_{ij}, and σ_s, we obtain the variation of q, which is given by

$$\Delta q = 2\left[\frac{b_{bs}}{(1+b_{bs})^2}\frac{\partial q}{\partial R_{bs}} - \frac{b_{ps}}{(1+b_{ps})^2}\frac{\partial q}{\partial R_{ps}}\right]\frac{\Delta e_s}{e_s} - \frac{1}{2}\sigma_s\frac{\partial q}{\partial \sigma_s}\frac{\Delta \alpha_s}{\alpha_s}$$

The sensitivity is defined by

$$S \equiv \frac{\Delta q}{q},$$

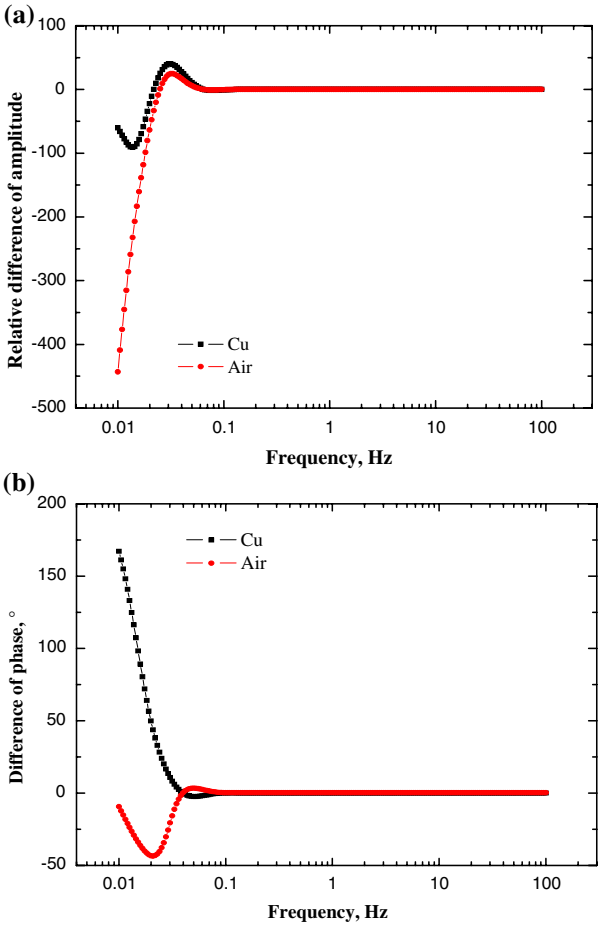

Fig. 6 Relative difference between the complete FPPE signal and the thermally thick approximation for water sample: (**a**) amplitude and (**b**) phase

The amplitude of S provides information on the percentage change in the measured voltage amplitude if the thermal parameters are varied. Using the mathematical expressions for $|q|$ and $|\Delta q|$, obtained previously, the absolute value of the sensitivity is given by

$$|S| \equiv \frac{1}{|q|}\left|2\left[\frac{b_{\mathrm{bs}}}{(1+b_{\mathrm{bs}})^2}\frac{\partial q}{\partial R_{\mathrm{bs}}} - \frac{b_{\mathrm{ps}}}{(1+b_{\mathrm{ps}})^2}\frac{\partial q}{\partial R_{\mathrm{ps}}}\right]\frac{\Delta e_{\mathrm{s}}}{e_{\mathrm{s}}} - \frac{1}{2}\sigma_{\mathrm{s}}\frac{\partial q}{\partial \sigma_{\mathrm{s}}}\frac{\Delta \alpha_{\mathrm{s}}}{\alpha_{\mathrm{s}}}\right|. \quad (19)$$

In the particular case of thermally thick samples,

$$|S| \equiv \frac{|\Delta q|}{|q|} = \left[\frac{2b_{\mathrm{ps}}}{(1+b_{\mathrm{ps}})^2}\frac{\Delta e_{\mathrm{s}}}{e_{\mathrm{s}}}\right]\frac{1}{|q|}\left|\frac{\partial q}{\partial R_{\mathrm{ps}}}\right|, \quad (20)$$

where the magnitude q is given by Eq. 18. From Eq. 17 the following expression is obtained,

$$\frac{\partial q}{\partial R_{\mathrm{sp}}} = \frac{\mathrm{e}^{\sigma_{\mathrm{p}} l_1} - R_{\mathrm{gp}}^2 \mathrm{e}^{-\sigma_{\mathrm{p}} l_1}}{\left(\mathrm{e}^{\sigma_{\mathrm{p}} l_1} - R_{\mathrm{sp}} R_{\mathrm{gp}} \mathrm{e}^{-\sigma_{\mathrm{p}} l_1}\right)^2}.$$

Then

$$\left|\frac{\partial q}{\partial R_{\mathrm{sp}}}\right| = \left[\frac{\sqrt{1 - \left(2R_{\mathrm{gp}}^2 \cos 2x\right) \mathrm{e}^{-2x} + R_{\mathrm{gp}}^4 \mathrm{e}^{-4x}}}{1 - \left(2R_{\mathrm{sp}} R_{\mathrm{gp}} \cos 2x\right) \mathrm{e}^{-2x} + R_{\mathrm{gp}}^2 R_{\mathrm{sp}}^2 \mathrm{e}^{-4x}}\right] e^{-x} \tag{21}$$

$$|q| = \sqrt{1 + \left(R_{sp} - R_{gp}\right)\left[\frac{(2\cos x)\,\mathrm{e}^{-x} + \left(R_{sp} - R_{gp}\right)\mathrm{e}^{-2x} - \left(2R_{sp} R_{gp} \cos x\right)\mathrm{e}^{-3x}}{1 - \left(2R_{sp} R_{gp} \cos 2x\right)\mathrm{e}^{-2x} + R_{sp}^2 R_{gp}^2 \mathrm{e}^{-4x}}\right]} \tag{22}$$

In Fig. 7, the numerical simulations of the sensitivity, given by Eq. 19, are shown. In this case the thermal effusivity of the sample is changed with respect to the corresponding value for water. The changes in the thermal effusivity have been parametrized in the form $\Delta e = (1 - \chi) e_{\mathrm{w}}$, where e_{w} is the thermal effusivity of water. In this case, χ has been given the following values 0.01, 0.05, 0.10, 0.50, and 0.99. As can be observed in Fig. 7, for the sensitivity graph, the signal has its maximum sensitivity at very low frequencies and decreases when the frequency increases, and the change in sensitivity is proportional to the change in thermal effusivity. It can also be observed in Fig. 7 that for large changes in thermal effusivity, the sensitivity decreases dramatically when the frequency increases. This can be interpreted that, at low frequencies, the PPE method is well suited to study small changes in thermal properties.

5 Experimental

The relative changes between amplitudes is given by

$$\eta = \left(1 - \frac{|q\,(\Delta e)|}{|q\,(e_{\mathrm{w}})|}\right) \times 100,$$

where $q(\Delta e)$ is the amplitude obtained when the thermal effusivity is varied, and $q(e_{\mathrm{w}})$ is the amplitude for the value when is no variation in the thermal effusivity. Figure 8 shows the results for the variation of the relative changes of amplitude when the parameters measuring the variation of the thermal effusivity are $\chi = 0.01$, 0.05, and 0.10. It can be observed in Fig. 8 that in the range from 0.1 to 10 Hz, the relative difference of amplitude is less than the relative change of effusivity.

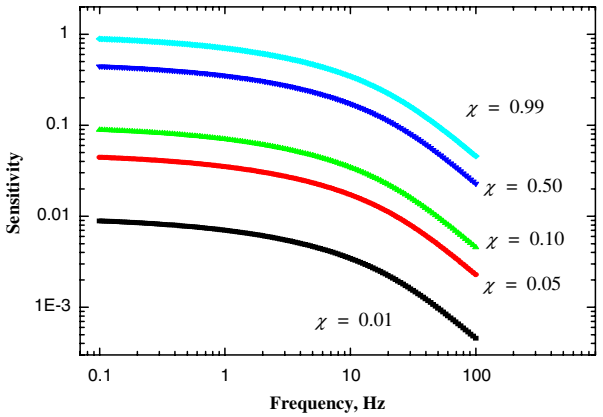

Fig. 7 Numerical simulation of the sensitivity. FPPE amplitude signal has its maximum sensitivity at very low frequencies and decreases when the frequency increases

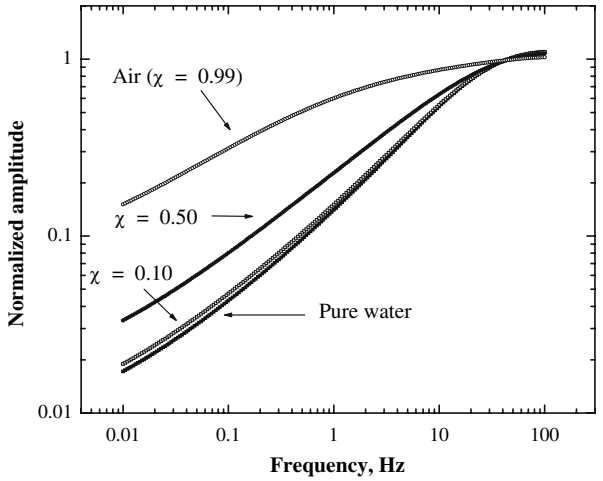

Fig. 8 Variation of the relative changes of the normalized amplitude as a function of frequency. Numbers for χ, close to each curve, represent the percentage variation of the thermal effusivity

The experimental results for the inverse of the signal-to-noise ratio (1/SNR) as a function of the frequency of modulation and for the two measurements modes, current and voltage, are presented in Fig. 9. The sample used was water. The inverse of the signal-to-noise ratio is used because, for any measurement, this parameter provided a contribution to the experimental error. Comparing the 1/SNR and the relative changes of the amplitudes, it can be observed that 1/SNR is a maximum at low frequencies, where the sensitivity is high. At 0.2 Hz, the contribution to the uncertainty is about of 10% of the signal. From 0.2 to 1.0 Hz, 1/SNR decreases and its contribution to the uncertainty is about 1%. With this uncertainty it is impossible to detect changes below $\chi = 0.05$, or changes in the effusivity below 5%. Due to the fact that, in any

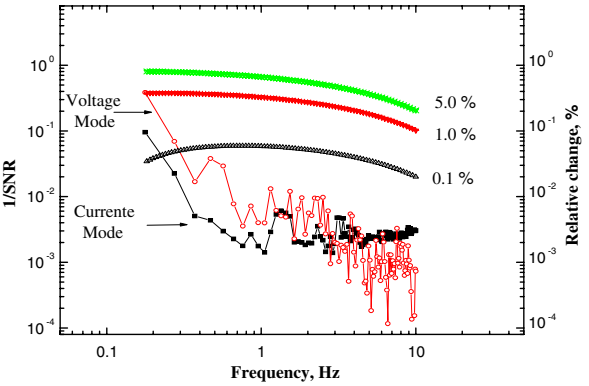

Fig. 9 Inverse of the signal-to-noise ratio and the relative difference of FPPE amplitude as a function of the frequency. In the signal-to-noise ratio experiments, the sample used was water; for the simulation, the thermal effusivity has been changed by 0.1%, 1.0%, and 5.0%

experiment, the noise is only one part of the uncertainties, we cannot detect changes in the thermal effusivity below to 10%.

6 Conclusions

In this article, two metrological aspects of the auto-normalized front photopyroelectric technique for thermal effusivity measurements in liquids that limit the accuracy in the measurements of the thermal effusivity have been explored. It has been demonstrated that the sensitivity shows a strong dependence on frequency, and at low frequencies, the change of sensitivity is equal to the change of the thermal effusivity in the frequency range from 0.01 to 0.05 Hz, decreasing up to 70% if the frequency is increased to 10 Hz.

Comparing the inverse of the signal-to-noise ratio, it is shown that the front photopyroelectric technique is a very good tool to measure the thermal effusivity and its variations, if the thermal effusivity has been changed more than 10%.

Acknowledgments This work was partially supported by CONACyT under Grant No. SEP-2003-C02–44058, and by CONCyTEG, Project No. 06–16-K117–99 A02.

References

1. A. Mandelis, M.M. Zver, J. Appl. Phys. **57**, 4421 (1985)
2. M. Chirtoc, G. Mihailescu, Phys. Rev B **40**, 9606 (1989)
3. A. Mandelis, F. Care, K.K. Chan, L.C.M. Miranda, Appl. Phys. A **51**, 387 (1985)
4. P.K. John, L.C.M. Miranda, A.C. Rastogi, Phys Rev. B **34**, 4342 (1986)
5. D. Dadarlat, M. Chirtoc, C. Nematu, R.M. Candea, D. Bicanic, Phys. Status Solidi **121**, K23 (1990)
6. D. Dadarlat, D. Bicanic, H. Visser, F. Mercuri, A. Frandas, J. Amer. Oil Chem. Soc., Part I, **72**, 273 (1995); Part II, **72**, 281 (1995)
7. Manual of the Piezo-Films, http://www.msiusa.com
8. D. Almond, P. Patel, *Photothermal Science and Techniques* (Chapman & Hall, London, 1996)
9. E.H. Bentefour, C. Glorieux, M. Chirtoc, J. Thoen, Rev. Sci. Instrum. **74**, 811 (2003)